

## Ground-state Gamow-Teller strength in $^{64}\text{Ni}(n,p)^{64}\text{Co}$ cross sections at 90–240 MeV

A. Ling,<sup>(1)</sup> X. Aslanoglou,<sup>(2)</sup> F. P. Brady,<sup>(3)</sup> R. W. Finlay,<sup>(2)</sup> R. C. Haight,<sup>(1)</sup> C. R. Howell,<sup>(4)</sup>  
 N. S. P. King,<sup>(1)</sup> P. W. Lisowski,<sup>(1)</sup> B. K. Park,<sup>(2)</sup> J. Rapaport,<sup>(2)</sup> J. L. Romero,<sup>(3)</sup> D. S. Sorenson,<sup>(1,3)</sup> W. Tornow,<sup>(4)</sup>  
 and J. L. Ullmann<sup>(1)</sup>

<sup>(1)</sup>Los Alamos National Laboratory, Los Alamos, New Mexico 87545

<sup>(2)</sup>Ohio University, Athens, Ohio 45701

<sup>(3)</sup>University of California, Davis, California 95616

<sup>(4)</sup>Duke University and Triangle Universities Nuclear Laboratory, Durham, North Carolina 27706

(Received 9 August 1991)

Cross sections have been measured for the reaction  $^{64}\text{Ni}(n,p)^{64}\text{Co}$  at laboratory angles between  $0^\circ$  and  $10^\circ$  for incident neutron energies from 90 to 240 MeV. The ground-state cross sections together with the  $\beta^-$  decay  $ft$  value for the transition  $^{64}\text{Co}(\text{g.s.}) \rightarrow ^{64}\text{Ni}(\text{g.s.})$  are used to normalize the  $q=0$  differential cross section in units of mb/sr per unit Gamow-Teller (GT) strength. This is the first absolute measurement of the  $A(n,p)$  unit cross section for a nucleus in the  $(fp)$  shell, and it may be used to calibrate the GT strength measured in other  $(n,p)$  reactions of similar mass nuclei. Since the  $(e^-, \nu_e)$  channel involves the same nuclear matrix element as the  $(n,p)$  channel, knowledge of GT strength in these nuclei is important for supernova modeling codes which depend on knowledge of  $e^-$  capture rates of  $(fp)$ -shell nuclei to determine parameters of stellar core collapse.

### I. INTRODUCTION

An important process occurring in presupernova stars is  $e^-$  capture on free protons and nuclei [1–3]. The rate at which this process occurs determines the number of leptons per nucleon,  $Y_e$ , at the neutrino trapping point. This in turn determines the inner core mass and perhaps the strength of the outgoing shock wave that forms when the core bounces. Knowledge of the behavior of  $Y_e$  with time is crucial to the understanding of the supernova phenomenon since it appears in the equation of state [4–9]. At the beginning of stellar collapse nuclear fusion fuels have been depleted, leaving the star with a center made up of nuclei in the iron region. The  $e^-$  capture rates for  $(fp)$ -shell nuclei are therefore important in understanding the behavior of the star from the moment it becomes dynamically unstable.

Since  $e^-$  capture and the charge-exchange reaction  $(n,p)$  between same initial and final states are both  $T_0 \rightarrow T_0 + 1$  transitions involving the same nuclear matrix element, the  $(n,p)$  reaction can be used to provide the input required to calculate  $e^-$  capture rates. Specifically, the  $e^-$  capture rate  $\lambda^{if}$ , for a nucleus going from an initial state  $i$  to a final state  $f$  is proportional to the Gamow-Teller strength [10]  $B_{\text{GT}}^{if}$ :

$$\lambda^{if} = G(\rho, T, Y_e) B_{\text{GT}}^{if}. \quad (1)$$

$G$  is a function that depends on  $Y_e$ , the density  $\rho$ , and temperature  $T$  of the star, as well as specific features of the particular initial and final states such as the spin, excitation, and nuclear partition function of the initial nucleus and the mean-square energy of the emitted neutrino.  $B_{\text{GT}}^{if}$  is given by [11]

$$B_{\text{GT}}^{if} = \frac{1}{2J_i + 1} \left| \left\langle f \left\| \sum_k \sigma_k \tau_k^\pm \right\| i \right\rangle \right|^2. \quad (2)$$

Once  $B_{\text{GT}}^{if}$  for a particular transition is known, the corresponding  $e^-$  capture rate  $\lambda^{if}$ , for that transition can be calculated for a specific density and temperature in a stellar core.

Nucleon charge-exchange reactions can be used to determine the Gamow-Teller strength. As indicated in Ref. [12], the unit cross section for Gamow-Teller transitions  $\hat{\sigma}_{\text{GT}}(E, A)$  relates  $B_{\text{GT}}^{if}$  to the differential cross section for  $(n,p)$  or  $(p,n)$  reactions:

$$\sigma(q, \omega) = \hat{\sigma}_{\text{GT}}(E, A) F(q, \omega) B_{\text{GT}}^{if}. \quad (3)$$

The function  $F(q, \omega)$  gives the dependence of the cross section on momentum transfer  $q$  and energy loss  $\omega$ .  $F(q, \omega)$  is equal to unity in the limit  $(q, \omega) \rightarrow 0$ . The constants  $\hat{\sigma}_{\text{GT}}(E, A)$  and  $B_{\text{GT}}^{if}$  give the absolute magnitude of the cross section. The value of  $\hat{\sigma}_{\text{GT}}(E, A)$  is empirically determined from extrapolating forward-angle Gamow-Teller cross sections to  $(q, \omega) = 0$  for cases in which there exists a  $\beta^-$  or  $\beta^+$  decay between the initial and final nuclear states. Thus  $\hat{\sigma}_{\text{GT}}(E, A)$  is determined from measured angular distributions for transitions with a known  $B_{\text{GT}}^{if}$ . However, calculated values of  $\hat{\sigma}_{\text{GT}}(E, A)$  have been seen to have a smooth  $A$  dependence [12]. Thus, when values of  $\hat{\sigma}_{\text{GT}}(E, A)$  in a given mass region are known, measurements of forward-angle  $(n,p)$  or  $(p,n)$  cross sections extrapolated to  $(q, \omega) = 0$  should allow values of  $B_{\text{GT}}^{if}$  to be determined for cases in which there is no  $\beta^-$  or  $\beta^+$  decay between initial and final nuclear states.

The data presented here allow a value for  $\hat{\sigma}_{\text{GT}}$  in the  $(fp)$  shell to be calculated from the Gamow-Teller

strength for the  $\beta^-$  decay  ${}^{64}\text{Co}(\text{g.s.}) \rightarrow {}^{64}\text{Ni}(\text{g.s.})$ . This decay with  $\log(ft) = 4.27 \pm 0.02$  [13] is the strongest  $\beta^-$  decay to the ground state of a stable nucleus in the ( $fp$ ) shell. The next strongest  $\beta^-$  decay is the transition  ${}^{69}\text{Zn}(\text{g.s.}) \rightarrow {}^{69}\text{Ga}(\text{g.s.})$  which has a  $\log(ft) = 4.48 \pm 0.01$  [14]. The  $\beta^-$  decay  ${}^{66}\text{Ni}(\text{g.s.}) \rightarrow {}^{66}\text{Cu}(\text{g.s.})$  has a  $\log(ft) = 4.17$  [15], but because  ${}^{66}\text{Cu}$  is short lived, it cannot be easily used as a target. Other  $\beta^-$  decays that one could conceive of using to calibrate Gamow-Teller strength in the ( $fp$ ) shell have strengths that are weaker by nearly an order of magnitude. Thus the  $\beta^-$  decay  ${}^{64}\text{Co}(\text{g.s.}) \rightarrow {}^{64}\text{Ni}(\text{g.s.})$  is the best decay to use for calibrating GT strength in the ( $fp$ ) shell since it is the strongest, best known  $\beta^-$  decay in this mass region.

The  $\beta^-$  strength is obtained from the relation [12]

$$B_{\text{GT}}^{\beta^-} = \frac{6166 \pm 2}{(g_A/g_V)^2 ft} \quad (4)$$

The constant 6166 reflects the choice of the vector coupling constant recommended by Wilkinson [16]. For  $g_A/g_V$  we have used the value  $g_A/g_V = 1.260 \pm 0.008$  [17] obtained in free neutron decay. The value for  $ft$  is calculated from the measured half-life and branching ratio. Rahkonen and Kantele [18] determined the  ${}^{64}\text{Co}$  half-life to be  $t_{1/2} = 0.30 \pm 0.03$  s with a branching ratio of  $90 \pm 5\%$ . The value of  $\log(f) = 4.749 \pm 0.006$  was obtained from Ref. [19]. Since  $\beta^-$  decay of  ${}^{64}\text{Co}(\text{g.s.})$  and the reaction  ${}^{64}\text{Ni}(n,p){}^{64}\text{Co}(\text{g.s.})$  have opposite initial and final states, detailed balance can be used to relate the Gamow-Teller strengths for the two processes:

$$B_{\text{GT}}^{np} = \frac{(2J_f + 1)}{(2J_i + 1)} B_{\text{GT}}^{\beta^-} = 0.62_{-0.04}^{+0.03}, \quad (5)$$

where  $J_i$  and  $J_f$  are the spins of the initial and final states in the ( $n,p$ ) reaction. It is this value of  $B_{\text{GT}}^{np}$  together with the differential cross-section measurements presented here for the reaction  ${}^{64}\text{Ni}(n,p){}^{64}\text{Co}(\text{g.s.})$  that allow  $\hat{\sigma}_{\text{GT}}$  to be calculated and thus an empirical calibration point in the ( $fp$ ) shell is established.

Measurements of ( $n,p$ ) reaction cross sections on other ( $fp$ )-shell nuclei and their corresponding GT strength distributions have been reported by several authors

[20–23]. The empirical values of the unit cross section presented here may therefore be compared with those used in Refs. [20–23] to express the GT strength distribution of these nuclei in units of GT strength.

## II. EXPERIMENTAL METHOD

Differential cross sections were measured in the angular range  $0^\circ$ – $10^\circ$  for incident neutron energies 90–240 MeV using the WNR white neutron source at LAMPF [24]. The data presented here was obtained over a two-week period. A multitarget array and a system of wire chambers for target identification, drift chambers, CsI(Tl) counters, and a  $\Delta E$  scintillator were set up on the  $15^\circ$  left flight path at 90 m from the neutron production target [25]. The detector system is shown schematically in Fig. 1. Unwanted events due to charged particles in the incident beam of spot size  $10 \times 10$  cm<sup>2</sup> were tagged by two veto chambers placed in front of the target chamber assembly. The target chamber assembly consisted of four wire chambers with a  $7.5 \times 5.0$  cm<sup>2</sup> nickel target (145.6 mg/cm<sup>2</sup>) enriched to 97.93% in  ${}^{64}\text{Ni}$  placed in the second target location. A CH<sub>2</sub> (76.1 mg/cm<sup>2</sup>) target was placed downstream in the fourth target location for normalization purposes. Protons from the ( $n,p$ ) reaction near  $0^\circ$  were swept by a 0.5-T magnet into a rectangular calorimeter wall 27.9 cm tall by 50.0 cm wide consisting of 15 CsI(Tl) counters each of dimensions  $8.9 \times 8.9 \times 15.2$  cm<sup>3</sup>. These counters gave the energies of the detected particles which were then corrected for energy loss in all material traversed by the particles. The energy resolution of the detected protons ranged from 1.5 at low energies to 2.4 MeV at the higher energies. A large plastic scintillator 0.5 cm thick was placed in front of the CsI(Tl) array to obtain the incident neutron energy from time of flight and was also used as a  $\Delta E$  detector.

The efficiency of the target chambers ranged from 92% to 98%, and therefore the excitation spectra for targets 2, 3, and 4 had to be corrected for misidentified events, i.e., events incorrectly associated with a target downstream of the true target. This was done in the following manner. A percentage of the excitation spectra of all targets upstream of a specific target was subtracted from the ex-

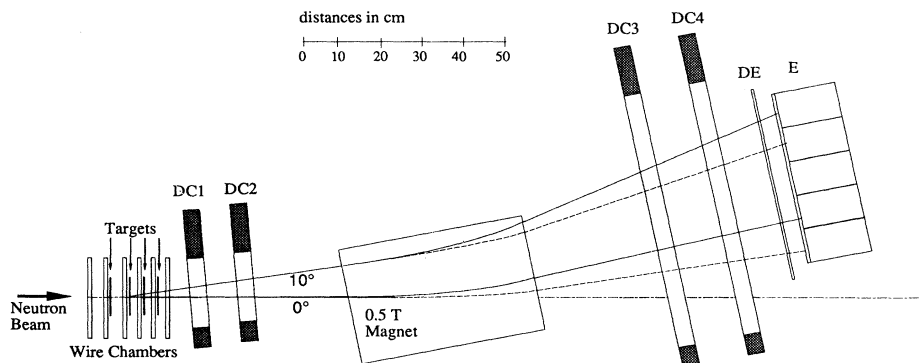


FIG. 1. The detector system at the end of the 90-m flight path used to obtain the data presented in this work.

citation spectrum of that target. To account for the differences in  $(n,p)$  reaction  $Q$  values of the targets, all excitation spectra were linearly shifted in excitation energy to correspond to a ground-state  $Q$  value of zero before any subtractions were performed. The percentage of an upstream target excitation spectrum subtracted was determined from the inefficiencies of all target chambers upstream of the target of interest. The corrected number of counts in each channel of an excitation spectrum for target  $T_i$ ,  $N_c(T_i)$ , were then obtained from the uncorrected shifted spectrum,  $N(T_i)$ , according to the relation

$$N_c(T_i) = N(T_i) - \sum_{j=1}^{i-1} N_c(T_j) \prod_{k=j}^{i-1} \bar{\epsilon}(T_k), \quad i=2,3,4, \quad (6)$$

where  $\bar{\epsilon}(T_k)$  is the inefficiency of target chamber  $k$ . The inefficiencies of all target chambers were determined from veto events. Since no targets were upstream of target 1, no correction was applied to the target 1 excitation spectra. After the excitation spectra were corrected in this manner, they were shifted in excitation energy to their original positions. Up to about 7% of the target excitation spectrum from target 1 was subtracted from the  $^{64}\text{Ni}$  excitation spectrum for each energy and angle range. The resulting corrected excitation spectra are shown in Figs. 2, 3, and 4 for the laboratory angular ranges  $0-4^\circ$ ,  $4-6^\circ$ , and  $6-10^\circ$ , respectively.

The angle binning was selected to be  $0-4^\circ$ ,  $4-6^\circ$ , and  $6-10^\circ$  and the energy binning  $90-120$ ,  $120-160$ ,  $160-200$ , and  $200-240$  MeV. These ranges were chosen in order to evenly distribute statistics among the cross-section spectra. The strong forward peak at 0 MeV excitation contains the GT strength associated with the  $\beta^-$  decay of  $^{64}\text{Co}(g.s.)$  to the ground state of  $^{64}\text{Ni}$ . As can be seen from the spectra, the number of counts in this peak is quite low, particularly at the larger angles. The presence of the "continuum" cross section representing the excitation in the region of the high density of states further complicates the task of determining the number of counts in the spectra associated with the peak. Under these circumstances, the standard methods of peak extraction work marginally at best. Therefore a nonstandard but simple and straightforward approach was used to determine the number of counts in the peaks at 0 MeV excitation.

The procedure for obtaining the number of counts in the peaks was simply to fit one of the larger peaks in which complications from low statistics and "continuum" contamination are minimal and then use the fit parameters of this peak along with the measured resolution of the system as a guide to determine the characteristics of the peaks in the other spectra. This was done in the following manner. The peak in the spectrum for the energy range  $90-120$  MeV and the angular range  $0-4^\circ$  was fit with a  $\chi^2$  minimization routine [26] to a Gaussian

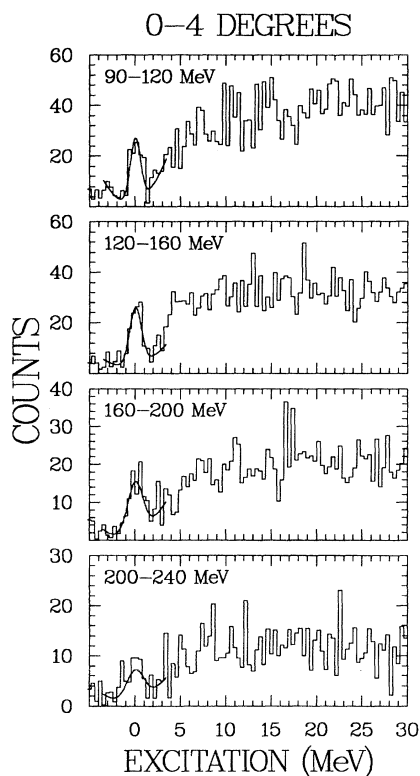


FIG. 2. Excitation spectra for the reaction  $^{64}\text{Ni}(n,p)^{64}\text{Co}$  from  $\theta_{\text{lab}}=0^\circ-4^\circ$ . Also shown is the fit described in the text for the peak at 0 MeV excitation.

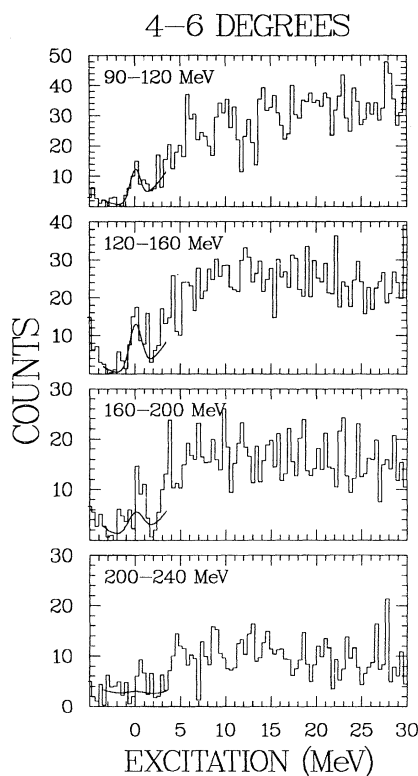


FIG. 3. Excitation spectra for the reaction  $^{64}\text{Ni}(n,p)^{64}\text{Co}$  from  $\theta_{\text{lab}}=4^\circ-6^\circ$ . Also shown is the fit described in the text for the peak at 0 MeV excitation.

representing the peak plus a quadratic term representing the part of the “continuum” under the peak. Since data taken with no targets in place provided background information with large statistical uncertainties, it was decided to represent the background with a constant term in fitting the peak, rather than subtract out the measured background from the spectrum. The fit of this peak near 0 MeV excitation gave a centroid of the Gaussian term of  $0.05 \pm 0.08$  MeV with a full width at half maximum (FWHM) equal to  $1.3 \pm 0.1$  MeV. The result that the centroid is very close to zero indicates that our calibration of excitation energy is in good agreement with the  $Q$  value [27] of  $-6.52 \pm 0.02$  MeV for the reaction  $^{64}\text{Ni}(n,p)^{64}\text{Co}(\text{g.s.})$  that was used in the kinematics to analyze our data.

The peaks for the other energy and angle ranges were fit in a similar manner but with the centroid fixed at 0.05 MeV and the standard deviation,  $\sigma$ , of the Gaussian held constant to the  $\sigma$  from the fit described above scaled to the resolution of the detector system for the specific energy and angular range. The resolution of the system was determined from the width of the hydrogen peaks of the target 4 excitation spectra. These values were used to scale the standard deviation parameters held constant in the fits to the 0-MeV excitation peak in the  $^{64}\text{Ni}(n,p)^{64}\text{Co}$  spectra according to the expression

$$\sigma(^{64}\text{Ni}, E, \theta) = \frac{1.3}{1.46} \sigma(\text{H}, E, \theta), \quad (7)$$

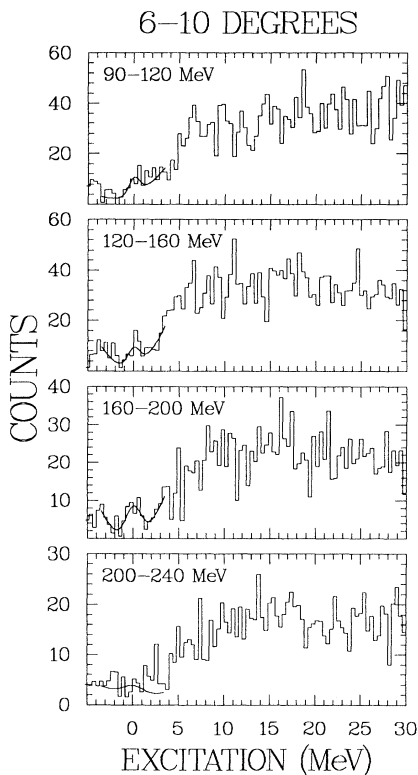


FIG. 4. Excitation spectra for the reaction  $^{64}\text{Ni}(n,p)^{64}\text{Co}$  from  $\theta_{\text{lab}} = 6^\circ - 10^\circ$ . Also shown is the fit described in the text for the peak at 0 MeV excitation.

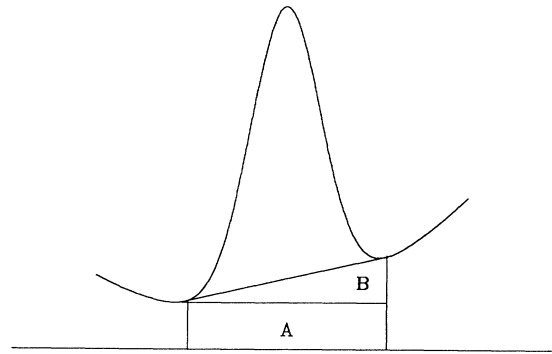


FIG. 5. Diagram showing the method used to extract the number of counts in the peak at 0 MeV excitation as described in the text.

where 1.3 is the full width at half maximum of the fitted peak for the energy range 90–120 MeV and the angular range  $0-4^\circ$  and 1.46 is the full width at half maximum of the hydrogen peak of target 4 for the same energy and angle range.

After each peak was fit, a diagram was drawn on each spectrum as shown in Fig. 5. Vertical lines were drawn from the fitted function to the  $x$  axis at  $\pm 3\sigma$ . The background represented by a constant is shown as the enclosed area labeled “A” in the figure. A triangle was then drawn to enclose the area “B.” Because the exact shape of the “continuum” under the peak is unknown, the triangle allows the extreme maximum and minimum contributions that the “continuum” might have on the peak area to be seen. If the “continuum” contributes significantly to the peak area, the most it could contribute would be the total area of B. If the “continuum” contributes very little, the least contribution would be no contribution at all, i.e., the area of B is taken as zero. Since the truth is somewhere in between the two extremes, we have taken the average and set the number of counts associated with the peak to be the total number of counts between  $\pm 3\sigma$ , less the area of A, less one-half the area of B.

The solid-angle acceptance for each target was determined from a Monte Carlo simulation. The simulation generated events that originated from different locations in each target and tracked the emerging protons through the detector system to the plane of the CsI(Tl) detector array. The ratio of events hitting the CsI(Tl) detectors to all events generated gave the solid-angle acceptance for a specific target and outgoing proton energy. The solid angle acceptance was then calculated as a function of excitation energy for each target and for the energy and angle bins specified above. The acceptance was averaged over the width of the peak at 0 MeV excitation and this was taken as the solid-angle acceptance for a given energy and angle bin.

The yield from the  $\text{H}(n,p)$  reaction of target 4, together with hydrogen cross sections calculated from the

TABLE I. Energy and angle centroids for the energy bins 90–120, 120–160, 160–200, and 200–240 MeV and the angle bins 0–4°, 4–6°, and 6–10°. Hydrogen cross sections used to normalize the neutron flux and  $^{64}\text{Ni}(n,p)^{64}\text{Co}$  cross sections measured for the peak at 0 MeV excitation.

Energy (MeV)	Angle (lab) (deg)	$d\sigma/d\Omega(\text{lab})\text{H}(n,p)$ (mb/sr)	$d\sigma/d\Omega(\text{c.m.})^{64}\text{Ni}(n,p)^{64}\text{Co}$ (mb/sr)
105.7±0.5	2.66±0.05	56.5	1.8±0.3
140.4±0.8	2.39±0.06	53.0	2.1±0.3
177.6±0.9	2.52±0.07	50.0	3.0±0.4
220.2±1.3	2.51±0.09	49.6	2.7±0.6
104.4±0.8	4.96±0.04	51.9	1.2±0.2
137.6±1.0	4.88±0.04	47.7	2.3±0.3
176.1±1.2	4.94±0.05	44.0	2.2±0.5
220.2±1.3	4.93±0.07	41.5	1.7±0.8
106.2±0.7	7.81±0.07	46.3	1.0±0.2
137.5±1.0	8.00±0.08	40.3	0.6±0.2
179.0±1.1	7.93±0.09	36.2	0.6±0.3
216.6±1.4	8.00±0.12	33.5	1.2±0.5

Arndt SM86 phase shifts [28], gave the flux of neutrons incident on the targets. The flux ranged from 9.0 neutrons  $\text{MeV}^{-1}\text{s}^{-1}\text{cm}^{-2}$  at 90 MeV to 2.4 neutrons  $\text{MeV}^{-1}\text{s}^{-1}\text{cm}^{-2}$  at 240 MeV. The phase-shift cross sections were interpolated to the energy and angle centroids of each bin and then used for normalizing the neutron flux. The energy and angle centroids of each bin were determined from gating on the 0-MeV excitation peak of the nickel target spectra and calculating the centroids of the energy and angle histograms. Table I lists these centroids along with the hydrogen cross sections used to normalize the data and the  $^{64}\text{Ni}(n,p)^{64}\text{Co}$  cross sections we have measured for the peak at 0 MeV excitation.

The experimental resolution in the present study was about 1.5 MeV and thus the proton peak observed at 0 MeV excitation may contain several states in addition to the ground state. Flynn and Garrett [27] have located 13 levels in  $^{64}\text{Co}$  below 2 MeV excitation energy via the  $^{64}\text{Ni}(t,^3\text{He})^{64}\text{Co}$  reaction with a 23.5-MeV triton beam. Some insight into how many of these are  $1^+$  states is provided by Runte *et al.* [29] who studied the  $\beta^-$  decay of  $^{64}\text{Fe}$  to  $^{64}\text{Co}$ . They report a  $Q_\beta$  value of 3.9 MeV and a 2.0-s half-life for  $^{64}\text{Fe}$ . Besides the ground-state transition, a weak transition to a state at 0.311 MeV is identified, in agreement with the state at  $0.296\pm 0.015$  MeV reported in Ref. [27]. Both the ground state and the 0.311-MeV state are assigned a spin-parity of  $1^+$ . We therefore believe that the yield observed in the  $^{64}\text{Ni}(n,p)^{64}\text{Co}$  reaction peak at 0 MeV excitation contains both Gamow-Teller transitions. However, Runte *et al.* [29] give the branching intensities of the  $\beta^-$  decay of  $^{64}\text{Fe}$  to the ground state and the 0.311-MeV state of  $^{64}\text{Co}$  to be 95% and 5% and the  $\log(ft)$  values to be 3.8 and 4.9, respectively. Thus, if the overlap of the  $^{64}\text{Ni}$  ground-state wave function and these  $1^+$  states of  $^{64}\text{Co}$  is similar to that of the  $^{64}\text{Fe}$  ground-state wave function and the same  $^{64}\text{Co}$   $1^+$  states, the contribution of the 0.311-MeV excited state to our result should be less than 10%.

### III. RESULTS AND CONCLUSION

Angular distributions for the proton groups centered at 0 MeV excitation for the reaction  $^{64}\text{Ni}(n,p)^{64}\text{Co}$  are shown in Fig. 6 for mean neutron energies 106, 139, 178, and 219 MeV, respectively.

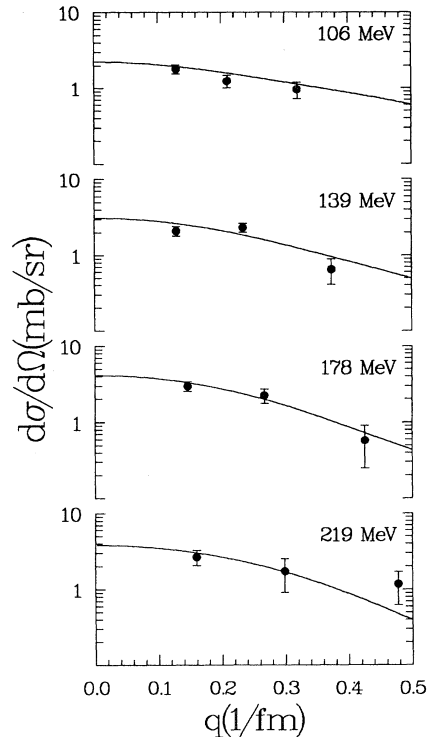


FIG. 6. Center-of-mass differential cross sections for the proton group observed at 0 MeV excitation in the reaction  $^{64}\text{Ni}(n,p)^{64}\text{Co}$  as a function of  $q$ . The solid line is a Gamow-Teller ground-state DWIA calculation multiplied by  $B_{GT}^{np}$  and normalized to the data. The normalization factors are  $0.67\pm 0.07$ ,  $0.70\pm 0.07$ ,  $0.93\pm 0.11$ , and  $0.72\pm 0.14$  for 106, 139, 178, and 219 MeV, respectively.

and 219 MeV. These energies were determined from the weighted means of the energies listed in Table I. Each distribution was used to normalize a Gamow-Teller distorted-wave impulse-approximation (DWIA) curve generated by the program DW81 for that energy [30]. We used the  $t$  matrices of Franey and Love [31] at 100, 140, 175, and 210 MeV and the Schwandt optical model parameters [32] as input to the program. Since Schwandt optical model parameters do not extend to our highest energy, we used the values of the parameters at 175 MeV as input to the DWIA calculation at 219 MeV. A five-particle-one-hole [ $\pi(f_{7/2})^{-1}\nu(f_{5/2})^5$ ] configuration was chosen with a  $Z$  coefficient [33] of  $(2j_i+1)^{-1/2} = 0.35355$ , where  $j_i = 7/2$ . The resulting DWIA curves were then normalized to the measured angular distributions and  $\hat{\sigma}_{GT}$  obtained from the relation

$$\hat{\sigma}_{GT} = \frac{N\sigma^{\text{DW81}}(\theta=0^\circ, q, \omega)}{B_{GT}^n} \left\{ \frac{\sigma^{\text{DW81}}(q=0, \omega=0)}{\sigma^{\text{DW81}}(\theta=0^\circ, q, \omega)} \right\}. \quad (8)$$

$N$  is the normalization factor and the quantity in braces is seen to be the function  $F(q, \omega)^{-1}$  by comparison with Eq. (3), evaluated at specific values of  $q$  and  $\omega$ . The program DW81 generates DWIA angular distributions down to  $\theta=0^\circ$  at some finite value of  $q$  and  $\omega$ . Thus the curves had to be extrapolated to  $q=0$  in order to obtain  $\sigma^{\text{DW81}}(q=0, \omega=0)$ . This was done by setting the  $Q$  value for the reaction equal to zero and running the program to get the shape of the curve from  $q=0$  to  $q(\theta=0^\circ)$ . The obtained values of  $N$  for 106, 139, 178, and 219 MeV are  $0.67 \pm 0.07$ ,  $0.70 \pm 0.07$ ,  $0.93 \pm 0.11$ , and  $0.72 \pm 0.14$ , respectively. The resulting normalized DWIA curves are shown in Fig. 6. The value of the normalized DWIA curve at  $q=0$  was used to calculate the unit cross section.

The Gamow-Teller unit cross sections along with the zero-degree cross sections and the distortion and momentum-transfer correction factor  $F(q, \omega)$  are listed in Table II. Shown in Fig. 7 is the unit cross section as a function of energy for the  $^{64}\text{Ni}(n,p)^{64}\text{Co}$  reaction using  $\sigma^{\text{DW81}}(q=0, \omega=0)$  normalized to the measured angular distributions by the procedure discussed above. Also shown and joined with a smooth line are DWIA calculations performed at the energies of the existing Love-Franey  $t$  matrices, 100, 140, 175, and 210 MeV, normalized with the average value of  $N$ . Unit cross sections obtained in the reaction  $^{58}\text{Ni}(p,n)$  are also shown for comparison [12,34,35].

TABLE II. Zero-degree cross sections for the 0-MeV excitation peak of the reaction  $^{64}\text{Ni}(n,p)^{64}\text{Co}$ . Gamow-Teller unit cross sections and the distortion and momentum transfer correction factor.

Energy (MeV)	$\sigma(\theta=0^\circ)$ (mb/sr)	$\hat{\sigma}_{GT}$ (mb/sr)	$F(q, \omega)$
$105.5 \pm 0.4$	$1.9 \pm 0.2$	$3.6 \pm 0.4$	0.86
$138.7 \pm 0.5$	$2.8 \pm 0.3$	$5.0 \pm 0.5$	0.90
$177.7 \pm 0.6$	$3.9 \pm 0.5$	$6.6 \pm 0.8$	0.94
$219.0 \pm 0.8$	$3.6 \pm 0.7$	$6.1 \pm 1.2$	0.95

The unit cross section may be expressed as [12]

$$\hat{\sigma}_{GT}(E) = K(E)N^D |J_{\sigma\tau}(q=0)|^2, \quad (9)$$

where  $K(E)$  is a kinematic factor,  $N^D$  is a distortion factor, and  $J_{\sigma\tau}(q=0)$  represents the volume integral of the central part of the effective nucleon-nucleon interaction, evaluated at  $q=0$ . The energy dependence of  $\hat{\sigma}_{GT}(E)$  arises mainly from the kinematic factor  $K(E)$  and the small energy variation of  $J_{\sigma\tau}(E)$ . Both effects can be represented by an exponential form [12] which we have parametrized for the energy range  $125 < E < 225$  MeV in the  $^{64}\text{Ni}(n,p)^{64}\text{Co}$  case as

$$\hat{\sigma}_{GT}(E) = 0.614 \times 10^{(0.83+0.0008E)} \text{ mb/sr}, \quad (10)$$

where  $E$  is the incident energy in MeV. The dotted line in Fig. 7 represents this parametrization. A similar form has been used [36] for the energy dependence of the unit cross section in  $p$ -shell nuclei. The large discrepancy observed for energies below 125 MeV may be attributed to the distortion factor. As the energy decreases, a lower fraction of nucleons participating in the Gamow-Teller resonance is excited which accounts for lower  $N^D$  values. The DW81 calculations reproduce this decrease quite well.

The work described here is the first absolute measurement of the Gamow-Teller unit cross section from the  $(n,p)$  reaction for an  $(fp)$ -shell nucleus. The unit cross sections obtained from  $(p,n)$  reactions show that general proportionality has a smooth  $A$  dependence and holds over a wide range of  $A$  with a few exceptions in odd mass

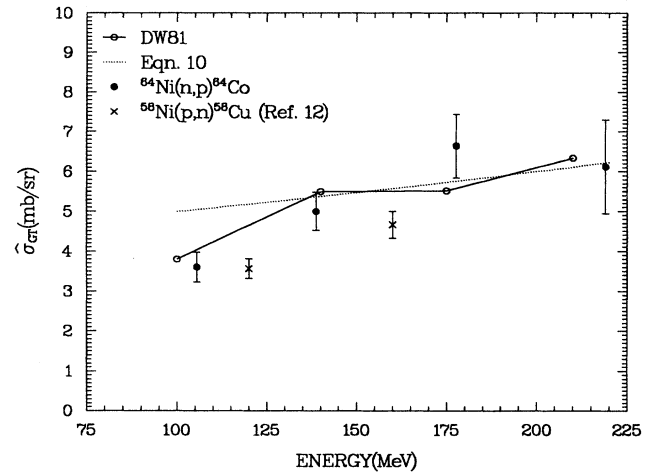


FIG. 7. The Gamow-Teller unit cross section as a function of energy for  $(fp)$ -shell nuclei. The errors shown for the reaction  $^{64}\text{Ni}(n,p)^{64}\text{Co}$  (g.s.) are statistical in nature only and do not include the uncertainty in the measured  $ft$  value or any uncertainties in the  $H(n,p)$  cross sections used to normalize the data. Also shown is a DWIA calculation at  $q=0$  performed at the energies of the existing Love-Franey  $t$  matrices, 100, 140, 175, and 210 MeV, normalized with the average value of the normalization factors of Fig. 6 and joined with a smooth line. The dotted line is a parametrization given by Eq. (10). Unit cross sections obtained in the reaction  $^{58}\text{Ni}(p,n)$  from Ref. [12] are also shown for comparison.

nuclei [12]. In contrast, the unit cross sections studied [37–39] so far in the  $p$ -shell nuclei  ${}^6\text{Li}$ ,  ${}^{12}\text{C}$ , and  ${}^{13}\text{C}$  for the  $(n,p)$  channel do not show any of the deviations from general proportionality that are apparent in the  $(p,n)$  reaction. It is seen that our measurements of  $\hat{\sigma}_{\text{GT}}$  are in good agreement with values of  $\hat{\sigma}_{\text{GT}}$  measured from  $(p,n)$  reactions on similar nuclei. Our values of  $\hat{\sigma}_{\text{GT}}$  appear to be slightly higher than those for  ${}^{58}\text{Ni}(p,n)$ , but this may be due to the contribution of the 0.311-MeV state discussed earlier as a possible small contaminant to our result. Thus the trend seen in GT strength observed in  $p$ -shell nuclei ( ${}^6\text{Li}$  and  ${}^{12}\text{C}$ ) from  $(n,p)$  and  $(p,n)$  reactions of data taken at WNR at LAMPF [37], Indiana University Cyclotron Facility [12,38,40–43], and TRIUMF [39,44] is again seen in the  $(fp)$  shell, i.e.,

$\hat{\sigma}_{\text{GT}}(n,p) \approx \hat{\sigma}_{\text{GT}}(p,n)$ . Our measurement of  $\hat{\sigma}_{\text{GT}}$  therefore allows calculations of  $e^-$  capture rates of  $(fp)$ -shell nuclei from measured  $(n,p)$  cross sections to be made with reasonable accuracy. The use of this information should then allow a more precise theoretical description of the supernova phenomenon to become possible.

#### ACKNOWLEDGMENTS

This work was supported in part by the U.S. Department of Energy under Contracts No. W-7405-ENG-36 and No. DE-AC05-76ER01067 and the National Science Foundation via Grants No. PHY87-22008 and No. PHY88-10220-03.

- 
- [1] J. Cooperstein and J. Wambach, Nucl. Phys. **A420**, 591 (1984).
- [2] G. M. Fuller, W. A. Fowler, and M. J. Newman, Astrophys. J. **252**, 715 (1982).
- [3] M. B. Aufderheide, Nucl. Phys. **A525**, 161 (1991).
- [4] H. A. Bethe, G. E. Brown, J. Applegate, and J. M. Lattimer, Nucl. Phys. **A324**, 487 (1979).
- [5] H. A. Bethe, Annu. Rev. Nucl. Part. Sci. **38**, 1 (1988).
- [6] J. Cooperstein, Nucl. Phys. **A438**, 722 (1985).
- [7] G. Baym, H. A. Bethe, and C. J. Pethick, Nucl. Phys. **A175**, 225 (1971).
- [8] H. A. Bethe, G. E. Brown, J. Cooperstein, and J. R. Wilson, Nucl. Phys. **A403**, 625 (1983).
- [9] H. A. Bethe, Rev. Mod. Phys. **62**, 801 (1990).
- [10] M. B. Aufderheide, G. E. Brown, T. T. S. Kuo, D. B. Stout, and P. Vogel, Astrophys. J. **362**, 241 (1990).
- [11] A. Bohr and B. M. Mottelson, *Nuclear Structure* (Benjamin, New York, 1969), Vol. I, p. 411.
- [12] T. N. Taddeucci, C. A. Goulding, T. A. Carey, R. C. Byrd, C. D. Goodman, C. Gaarde, J. Larsen, D. Horen, J. Rapaport, and E. Sugarbaker, Nucl. Phys. **A469**, 125 (1987).
- [13] M. L. Halbert, Nucl. Data Sheets **28**, 179 (1979); updated by B. Singh, *ibid.* **62**, 603 (1991).
- [14] M. R. Bhat, Nucl. Data Sheets **58**, 1 (1989).
- [15] N. J. Ward and F. Kearns, Nucl. Data Sheets **39**, 1 (1983).
- [16] D. H. Wilkinson, Nucl. Phys. **A377**, 474 (1982).
- [17] P. Bopp, D. Dubbers, L. Hornig, E. Klemt, J. Last, and H. Schütze, Phys. Rev. Lett. **56**, 919 (1986).
- [18] V. Rahkonen and J. Kantele, Phys. Fenn. **9**, 103 (1974).
- [19] On-line access program PHYSCO, National Nuclear Data Center, Brookhaven National Laboratory.
- [20] M. C. Vetterli *et al.*, Phys. Rev. C **40**, 559 (1989).
- [21] M. C. Vetterli *et al.*, Phys. Rev. Lett. **59**, 439 (1987).
- [22] W. P. Alford *et al.*, Nucl. Phys. **A514**, 49 (1990).
- [23] W. P. Alford, A. Celler, B. A. Brown, R. Abegg, K. Ferguson, R. Helmer, K. P. Jackson, S. Long, K. Raywood, and S. Yen, TRIUMF Report No. TRI-PP-90-81, 1990 (unpublished).
- [24] P. W. Lisowski, C. D. Bowman, G. J. Russell, and S. A. Wender, Nucl. Sci. Eng. **106**, 208 (1990).
- [25] D. S. Sorenson, Los Alamos Report No. LA-12061-T, 1991 (unpublished).
- [26] P. R. Bevington, *Data Reduction and Error Analysis for the Physical Sciences* (McGraw-Hill, New York, 1969), p. 212.
- [27] E. R. Flynn and J. D. Garrett, Phys. Lett. **42B**, 49 (1972).
- [28] R. A. Arndt and L. D. Roper, Scattering Analysis Interaction Dial-in (SAID) program, Virginia Polytechnic Institute, 1984 (unpublished).
- [29] E. Runte *et al.*, Nucl. Phys. **A441**, 237 (1985).
- [30] R. Schaeffer and J. Raynal, computer code DWBA70, Arizona State University, 1970 (unpublished); extended version: J. R. Comfort, computer code DW81, Arizona State University, 1984 (unpublished).
- [31] M. A. Franey and W. G. Love, Phys. Rev. C **31**, 488 (1985).
- [32] P. Schwandt, H. O. Meyer, W. W. Jacobs, A. D. Bacher, S. E. Vigdor, M. D. Kaitchuck, and T. R. Donoghue, Phys. Rev. C **26**, 55 (1982).
- [33] F. Petrovich, R. H. Howell, C. H. Poppe, S. M. Austin, and G. M. Crawley, Nucl. Phys. **A383**, 355 (1982).
- [34] J. Rapaport *et al.*, Phys. Lett. **119B**, 61 (1982).
- [35] J. Rapaport *et al.*, Nucl. Phys. **A410**, 371 (1983).
- [36] D. S. Sorenson *et al.* (unpublished).
- [37] D. S. Sorenson *et al.* (submitted to Phys. Rev. Lett.).
- [38] K. Wang, C. J. Martoff, D. Pocanic, W. J. Cummings, S. S. Hanna, R. C. Byrd, and C. C. Foster, Phys. Rev. C **38**, 2478 (1988).
- [39] K. P. Jackson *et al.*, Phys. Lett. **B 201**, 25 (1988).
- [40] C. A. Goulding, M. B. Greenfield, C. C. Foster, T. E. Ward, J. Rapaport, D. E. Bainum, and C. D. Goodman, Nucl. Phys. **A331**, 29 (1979).
- [41] G. L. Moake, L. J. Gutay, R. P. Scharenberg, P. T. Debevec, and P. A. Quin, Phys. Rev. C **21**, 2211 (1980).
- [42] J. Rapaport, T. Taddeucci, C. Gaarde, C. D. Goodman, C. C. Foster, C. A. Goulding, D. Horen, E. Sugarbaker, T. G. Masterson, and D. Lind, Phys. Rev. C **24**, 335 (1981).
- [43] J. Rapaport *et al.*, Phys. Rev. C **36**, 500 (1987).
- [44] J. W. Watson *et al.*, Phys. Rev. C **40**, 22 (1989).